

The Independent Pulsations of Jupiter’s Northern and Southern X-ray Auroras

W. R. Dunn^{1,2,3}, G. Branduardi-Raymont¹, L. C. Ray⁴, C. M. Jackman⁵, R. P. Kraft³, R. F. Elsner⁶, I. J. Rae¹, Z. Yao^{1,7}, M. F. Vogt⁸, G. H. Jones^{1,2}, G. R. Gladstone⁹, G. S. Orton¹⁰, J. A. Sinclair¹⁰, P. G. Ford¹¹, G. A. Graham¹, R. Caro-Carretero^{1,12}, A. J. Coates^{1,2}

¹ Mullard Space Science Laboratory, Department of Space & Climate Physics, University College London, Holmbury St. Mary, Dorking, Surrey RH5 6NT, UK

² The Centre for Planetary Science at UCL/Birkbeck, Gower Street, London, WC1E 6BT, UK

³ Harvard-Smithsonian Center for Astrophysics, Smithsonian Astrophysical Observatory, Cambridge, Massachusetts, USA

⁴ Department of Physics, Lancaster University, UK

⁵ Department of Physics and Astronomy, University of Southampton, Southampton, UK

⁶ NASA Marshall Space Flight Center, USA

⁷ Laboratoire de Physique Atmosphérique et Planétaire, Université de Liège, Liège, Belgium

⁸ Center for Space Physics, Boston University, USA

⁹ Space Science & Engineering Division, Southwest Research Institute, San Antonio, Texas, USA

¹⁰ Jet Propulsion Laboratory, California Institute of Technology, Pasadena, CA 91109, USA

¹¹ Kavli Institute for Astrophysics and Space Research, MIT, Cambridge MA, USA

¹² Escuela Técnica Superior de Ingeniería - ICAI, Universidad Pontificia Comillas, Madrid, Spain

Correspondence to William Dunn: w.dunn@ucl.ac.uk

Auroral hot spots are observed across the Universe at different scales¹ and mark the coupling between a surrounding plasma environment and an atmosphere. Within our own solar system, Jupiter possesses the only resolvable example of this large-scale energy transfer. Jupiter’s Northern X-ray aurora is concentrated into a hot spot, which is located at the most poleward regions of the planet’s aurora and pulses either periodically^{2,3} or irregularly^{4,5}. X-ray emission line spectra demonstrate that Jupiter’s Northern hot spot is produced by ~10s MeV high charge-state oxygen, sulphur and/or carbon ions^{4–6} undergoing charge exchange. Observations instead failed to reveal a similar feature in the South^{2,3,7,8}. Here, we report the existence of a persistent Southern X-ray hot spot. Surprisingly, this large-scale Southern auroral structure behaves independently of its Northern counterpart. Using XMM-Newton and Chandra X-ray campaigns, performed in May–June 2016 and March 2007, we show that Jupiter’s Northern and Southern spots each exhibit different characteristics, such as different periodic pulsations and uncorrelated changes in brightness. These observations imply that highly energetic, non-conjugate magnetospheric processes sometimes drive the polar regions of Jupiter’s dayside magnetosphere. This is in contrast with current models of X-ray generation for Jupiter^{9,10}. Understanding the behaviour and drivers of Jupiter’s pair of hot spots is critical to the use of X-rays as diagnostics of the wide-range of rapidly rotating celestial bodies that exhibit these auroral phenomena.

The XMM-Newton and Chandra X-ray Observatories conducted ~12 hour (1.2 Jupiter rotations) observations of Jupiter on 24th May (both XMM and Chandra) and 1st June (Chandra only) 2016 and a 5-hour observation (0.5 Jupiter rotations) on 3rd March 2007 (both Chandra and XMM - see supplementary material for analysis). At these times Jupiter's tilt provided excellent visibility of both Jupiter's Northern and Southern polar aurorae. The combination of Chandra's High Resolution Camera (HRC-2016 observations) and Advanced CCD Imaging Spectrometer (ACIS-2007 observation) and XMM-Newton's Reflection Grating Spectrometer (RGS) and European Photon Imaging Camera (EPIC) together provided high spatial and spectral resolution X-ray observations in the energy band 0.2-2.0 keV. The entire observable disk of Jupiter fits in both the Chandra-HRC and XMM-Newton-EPIC field of view, so that in 2016 both instruments provided continuous coverage of the planet for more than one Jupiter rotation and could observe both Northern and Southern aurora regions, as they rotated into view.

Both Chandra and XMM-Newton time-tag each X-ray photon, which, for Chandra HRC's high spatial resolution, allows Jupiter's X-ray emissions to be connected with the latitude and longitudes from which they originate. Unlike for Earth where observable surface features provide unique latitude-longitude coordinate identifiers, Jupiter's solid surface is not observable and its layers of cloud rotate around the planet at different rates. In order to apply a consistent coordinate reference frame to these observations, we therefore used the left-handed S3 coordinate system, which rotates with Jupiter's 9.925-hour rotation. Projections of the locations of these X-ray emissions on Jupiter's poles reveal that both Jupiter's Northern and Southern X-ray auroral emissions are concentrated into hot spots that persistently occur in the same S3 latitude-longitude locations (Fig. 1). These X-ray hot spots both occur poleward of Jupiter's main UV auroral oval, which is known to be generated by magnetospheric process(es) between 15 and 50 Jupiter Radii (R_J)¹¹. The Southern spot (poleward of -67° latitude and between 30° - 75° S3 longitude) occurs closer to its respective geographic pole than the Northern spot (60° - 75° latitude and 155° - 180° S3 longitude^{2,5}). This explains how, in previously published X-ray observations^{2,3}, unfavourable viewing meant the Southern hot spot was obscured.

Figure 2 shows overlaid lightcurves from the Northern and Southern hot spots to reveal the characteristic pulsations of each spot. At times when both spots are on Jupiter's observable disk (\sim CML 90° - 120°), these lightcurves show that the X-ray spots sometimes pulse together (e.g. minute 460, 24 May), but that more than 50% of their pulses are independent (e.g. minute 420-450 and 470-500 24 May). This means that knowledge of whether one hot spot brightens does not help to predict whether its counterpart also brightens.

The Northern X-ray spot has been observed to pulse either irregularly^{4,5} or with regular periods of 12, 26 or 40-45 minutes^{2,3}. In order to provide quantitative estimates of the periodicities in each of the hot spots for these observations, a Fourier transform was performed on the raw unsmoothed time series to produce power spectral density (PSD) plots (Fig. 3). These PSDs show that on both 24th May and 1st June 2016 the Southern spot pulsed with statistically significant regular periods of 9-11-min. Both Chandra and XMM-Newton independently observed this regular 9-11 minute period on 24 May. A Northern 12-min periodicity in the X-ray brightness was previously observed during a

magnetospheric compression³. The recurrence of a 9-12 min and 40-45-min^{2,3} period across multiple observations may suggest bi-modal regular periodicity.

Surprisingly, while the 9-11 min Southern spot period is highly statistically significant in both observations (probability of chance occurrence (PCO) 10^{-5} - 10^{-7}), the Northern spot pulsations show no significant 11-min period on 24th May and only a low-significance 12-min period (PCO 10^{-2}) on 1st June. The North does exhibit some lower significance (PCO $< 10^{-4}$) 5-8 min periods, but these are not consistent across hemispheres or instruments.

The periodicity is not the only characteristic that appears to behave independently for each spot during these observations. The lightcurves (Fig. 2) show that the brightnesses of the two spots are also uncorrelated. We observed 78 ± 9 X-ray photons from the Southern spot during the first CXO observation and 111 ± 11 X-ray photons during the second observation – a $\sim 40\%$ increase in X-ray emission. In contrast, we observed 298 ± 17 X-rays from the Northern spot during the first observation, but only 189 ± 14 X-rays during the second – emission decreased by $\sim 40\%$.

Analysis of the XMM-Newton EPIC spectra (supplementary information) shows that the dominant emissions from the Northern and Southern aurora are from precipitating ions of O^{7+} , 8^{+} and $S^{6+, \dots, 14+}$ and/or $C^{5+, 6+}$ and therefore relate to downward current regions^{9,10}. To more precisely identify the sources for these precipitating ions and the associated downward currents, we use a flux equivalence mapping model^{12,13} to connect magnetic field lines in the ionosphere with the equatorial magnetosphere (using the Northern Grodent Anomaly¹² and Southern VIP4¹⁴ models). Our Northern distribution (Fig. 4) matches the one observed previously^{3,8}, with the precipitating ions originating beyond 60 Jupiter Radii (R_J) and between 10:00 and 19:00 Magnetospheric Local Time (MLT). The Southern spot also maps beyond $60R_J$, but is concentrated between 10:00 and 14:00 MLT and it then rotates out of view before we have the opportunity to observe it mapping to later MLTs. If, as with the Northern spot, Southern X-rays continued to be triggered when the spot maps along the afternoon-dusk flank, this emission would be unobservable from Earth, addressing why fewer X-rays are almost always observed from the South¹⁵. This broader local time origin for the Northern spot may also explain the distinctive temporal signatures shown in Fig. 2 and 3, since more sources regions/process may be involved along the dusk flank.

Jupiter's magnetopause has a typical subsolar standoff distance of 60 - $90R_J$, depending on the solar wind dynamic pressure¹⁶. The flux equivalence mapping^{12,13} is calculated using magnetic field observations averaged over all solar wind conditions so that emission mapping beyond $60R_J$ could indicate ions precipitating on closed field lines from the outer magnetosphere and/or field lines that are open to the solar wind, depending on solar wind conditions at the time. Of the X-rays in each spot, 30-60% of photons mapped to locations beyond the modeled expanded magnetopause location and are thus not shown on Fig 4.

Currently, the favoured explanation for the Northern X-ray hot spot is that it is the signature of Jupiter's Northern cusp^{3,5,7,8} i.e. the dayside region of the magnetosphere that is open to the solar wind. It might therefore follow that Jupiter's Southern spot locates Jupiter's Southern cusp. For fast solar wind, X-rays are proposed to be generated in this cusp region by vortical flows from pulsed reconnection at the dayside

magnetopause⁹. These flows limit the downward currents into the ionosphere and produce ~MV field-aligned potential drops¹⁰. These potential drops can accelerate ~2 keV O²⁺ ions¹⁷ in the outer magnetosphere to the 16-32 MeV (1-2 MeV/amu) needed for Jupiter's atmosphere to strip electrons and produce the observed O⁶⁺ X-ray K-shell line emissions^{4,6,9}. If reconnection pulses occur at Jupiter's ~30-50 min Alfvén wave transit timescale it is suggested that this mechanism could also explain the 45-min X-ray periodicity⁹.

However, there are a varied set of challenges that need to be overcome in order for pulsed dayside reconnection to explain the generation of Jupiter's X-ray hot spots in the observation reported here: 1) the 9-12-min periodicity observed is on a shorter timescale than predicted; 2) for subsolar point reconnection, both poles should pulse periodically in-phase⁹, but the dominant periodicity in the South does not also dominate the Northern lightcurves (Fig. 3) and North-South pulsations often appear to be independent of one another (Fig. 2); 3) the overall brightness of the Northern spot appears to be uncorrelated to the overall brightness of the Southern spot, and 4) a more general challenge to the proposed pulsed reconnection mechanism is that it explains X-ray emissions during fast solar wind conditions, but previously X-rays have also been observed during slow solar wind conditions^{3,8}. To address these challenges, here we propose adaptations and alternative mechanisms to explain the observed soft X-ray hot spot emissions during these observations.

Differing pulsation periods for each pole could be produced by orientations of the Interplanetary Magnetic Field that do not favour subsolar reconnection⁹. At Saturn, tension associated with east-west motion of field lines during off-equatorial reconnection can produce transient non-conjugate enhancements in UV polar auroral brightness by disrupting field-aligned currents in the respective poles¹⁸.

High-latitude anti-parallel reconnection may also provide non-conjugacy. Lobe reconnection has been debated^{19,20} as Jupiter's dominant solar-wind reconnection process. This is predominantly because the planet's immense size, rapid rotation and internal plasma source lead to long relative timescales for return flows from an Earth-like Dungey cycle, and, under certain conditions, suppress dayside reconnection²¹. For high-latitude reconnection, reconnected/closing lobe field lines may travel equatorward across the cusp and into the dayside magnetosphere^{22,23}. This could explain the large spatial extent of the X-ray spots. Asymmetric high-latitude reconnection can also produce a persistent reconnection site over one pole and a moving reconnection site over the other pole. This may explain the contrasting regular 9-11 min X-ray period in the South and irregular pulsations in the North. Subsolar dayside reconnection can produce X-rays from high charge-state magnetosheath/solar wind ions (e.g. O⁷⁺) on open field lines, but these emissions are calculated to be orders of magnitude fainter than the total X-ray brightness observed^{9,10}. However, certain topologies of high-latitude reconnection may offer additional acceleration mechanisms, since stretched or twisted lobe/open field lines closing and dipolarising in the outer magnetosphere could energise ions through Fermi acceleration.

Kelvin Helmholtz Instabilities (KHIs) are perhaps one of the most important large-scale instabilities that occur in coronal, magnetospheric and astrophysical environments, transferring large quantities of energy, momentum and plasma between separate plasma regimes. They are also thought to occur at Jupiter's magnetopause^{21,24},

and offer an alternative mechanism capable of explaining the periodic X-ray signatures^{3,8}. For Earth's magnetosphere, KHIs can trigger magnetopause fluctuations and excite compressional ULF magnetic field oscillations and field line resonances, driving standing Alfvén waves in the ionosphere^{25,26}. At Jupiter, ULF waves have been observed with 10-20 min periodicity^{27,28}, the lower bound of which matches our 9-12 min X-ray pulsations. The periodicity of ULF oscillations depends on the magnitude of the magnetospheric cavity, velocity shear and thickness of the interaction boundary. At Jupiter, the size of the magnetosphere varies bi-modally between compressed and expanded states (respective standoff distances: 60-90R_J¹⁶). This could explain the bimodal 9-12-min and 40-45-min X-ray aurora periodicity. If the thickness of the magnetopause boundary and velocity shear were similar on 24th May and 1st June, then KHI-driven Alfvén waves could produce recurring periodicity. Moreover, KHIs could generate different brightening in each pole by driving oppositely-directed field-aligned currents in each hemisphere through Ampere's law. Traditional KH studies focus solely on the shear in the flow as the generation mechanism. However, magnetic field orientation, plasma characteristics and thickness of the magnetopause boundary all have critical roles to play in generating wave modes along the boundary. It is for these reasons that contrary to expectations from planetary rotation, KHIs are often observed along Earth²⁹ and Saturn³⁰'s dusk flank, as well as the dawn sector, where the velocity shear is largest. Indeed at larger velocity shears KHI may also be stabilized and hence switch off³⁰. The prevalence and locations of KHIs alongside the possibility of KHI generated ~MeV/amu acceleration required for the observed X-ray signatures remain to be fully explored at Jupiter. However, wave-particle interactions, KHI-driven reconnection and/or modulation of current systems and their associated potential drops are all possible acceleration mechanisms.

The Southern X-ray spot rotates out of view while the Northern spot rotates into view, so that both are observable simultaneously only when they approach opposite limbs of Jupiter's observable disk. If the two spots are globally driven, then arguably the simplest explanation for the North-South differences is that magnetospheric conditions changed with time and damped the 11-min Southern period. Whether the differences are due to changes with time or due to differing polar dynamics both auroral spots are fixed in the planet's rotating coordinate system, so localised magnetic conditions may also play some part in ensuring ~MeV/amu ion acceleration is produced only in the hot spots and not in any other auroral region.

These findings also highlight possible multi-wavelength connections for Jupiter's aurora. UV polar auroral flares³¹ sometimes coincide with X-ray brightenings⁵ and, like the X-ray pulsations, quasi-periodically enhance on a ~10 min timescale³². Bright infrared auroral hot spots are also co-located with the X-ray hot spots, which may suggest that the pulses of ~MeV/amu ion precipitation, and their associated drivers, provide an important heating mechanism for Jupiter's stratosphere down to the 10-mbar pressure level³³.

The independent behaviour of Jupiter's pair of soft X-ray hot spots during these observations raises fundamental questions about what processes at rapidly rotating magnetospheres produce these aurorae. For Jupiter, the precipitating ion spectral signatures suggest that the spots locate Jupiter's downward currents¹⁰ and may identify the Northern and Southern Cusps⁹. However, the observed distinctive behaviour could be indicative of non-equatorial reconnection, magnetopause-driven ULF waves, tail

reconnection or local magnetic conditions at each polar region. Over the coming 2 years, X-ray observing campaigns in conjunction with NASA's Juno mission will offer the opportunity to determine whether the independent behaviour that we report here is commonplace or is unique to the observations presented here. Critically, they will help to identify the magnetospheric conditions and auroral processes that are able to generate Jupiter's highest-energy emissions and the seemingly independent behaviour of the Northern and Southern soft X-ray hot spots.

References

1. Hallinan, G. *et al.* Magnetospherically driven optical and radio aurorae at the end of the stellar main sequence. *Nature* **523**, 568–571 (2015).
2. Gladstone, G. R. *et al.* A pulsating auroral X-ray hot spot on Jupiter. *Nature* **415**, 1000–1003 (2002).
3. Dunn, W. R. *et al.* The impact of an ICME on the Jovian X-ray aurora. *J. Geophys. Res. A Space Phys.* **121**, 2274–2307 (2016).
4. Branduardi-Raymont, G. *et al.* A study of Jupiter's aurorae with XMM-Newton. *Astron. Astrophys.* **463**, 761–774 (2007).
5. Elsner, R. F. *et al.* Simultaneous Chandra X ray Hubble Space Telescope ultraviolet, and Ulysses radio observations of Jupiter's aurora. *J. Geophys. Res. Space Phys.* **110**, 1–16 (2005).
6. Kharchenko, V., Bhardwaj, A., Dalgarno, A., Schultz, D. R. & Stancil, P. C. Modeling spectra of the north and south Jovian X-ray auroras. *J. Geophys. Res. Space Phys.* **113**, 1–11 (2008).
7. Branduardi-Raymont, G. *et al.* Spectral morphology of the X-ray emission from Jupiter's aurorae. *J. Geophys. Res. Space Phys.* **113**, 1–11 (2008).
8. Kimura, T. *et al.* Jupiter's X-ray and EUV auroras monitored by Chandra, XMM-Newton, and Hisaki satellite. *J. Geophys. Res. Space Phys.* **121**, 2308–2320 (2016).
9. Bunce, E. J., Cowley, S. W. H. & Yeoman, T. K. Jovian cusp processes: Implications for the polar aurora. *J. Geophys. Res. Space Phys.* **109**, 1–26 (2004).
10. Cravens, T. E. *et al.* Implications of Jovian X-ray emission for magnetosphere-ionosphere coupling. *J. Geophys. Res. Space Phys.* **108**, 1–12 (2003).
11. Cowley, S. W. H. & Bunce, E. J. Origin of the main auroral oval in Jupiter's coupled magnetosphere-ionosphere system. *Planet. Space Sci.* **49**, 1067–1088 (2001).
12. Grodent, D. *et al.* Auroral evidence of a localized magnetic anomaly in Jupiter's northern hemisphere. *J. Geophys. Res. Space Phys.* **113**, 1–10 (2008).
13. Vogt, M. F. *et al.* Improved mapping of Jupiter's auroral features to magnetospheric sources. *J. Geophys. Res. Sp. Phys.* **116**, 1–24 (2011).
14. Connerney, J. E. P., Acuña, M. H., Ness, N. F. & Satoh, T. New models of Jupiter's magnetic field constrained by the Io flux tube footprint. *J. Geophys. Res.* **103**, 11929–11939 (1998).
15. Waite, J. H. *et al.* ROSAT observations of the Jupiter aurora. *J. Geophys. Res.* **99**, 799–809 (1994).
16. Joy, S. P. *et al.* Probabilistic models of the Jovian magnetopause and bow shock locations. *J. Geophys. Res. Space Phys.* **107**, 1–17 (2002).
17. Bagenal, F. Empirical model of the Io plasma torus: Voyager measurements. *J. Geophys. Res.* **99**, 11043 (1994).
18. Meredith, C. J., Cowley, S. W. H., Hansen, K. C., Nichols, J. D. & Yeoman, T. K. Simultaneous conjugate observations of small-scale structures in Saturn's dayside ultraviolet auroras: Implications for physical origins. *J. Geophys. Res. Space Phys.* **118**, 2244–2266 (2013).
19. McComas, D. ~J. & Bagenal, F. Jupiter: A fundamentally different magnetospheric interaction with the solar wind. *Geophys. Res. Lett.* **34**, 1–5 (2007).
20. Cowley, S. W. H., Badman, S. V., Imber, S. M. & Milan, S. E. Comment on 'Jupiter: A fundamentally different magnetospheric interaction with the solar wind' by D. J. McComas and F. Bagenal. *Geophys. Res. Lett.* **35**, 1–3 (2008).
21. Desroche, M., Bagenal, F., Delamere, P. A. & Erkaev, N. Conditions at the expanded Jovian magnetopause and implications for the solar wind interaction. *J. Geophys. Res. Space Phys.* **117**, 1–18 (2012).
22. Lockwood, M. & Moen, J. Reconfiguration and closure of lobe flux by reconnection during northward IMF: possible evidence for signatures in cusp/cleft auroral emissions. *Ann. Geophys.*

- 17, 996–1011 (1999).
23. Fuselier, S. A., Trattner, K. J., Petrinec, S. M. & Lavraud, B. Dayside magnetic topology at the Earth's magnetopause for northward IMF. *J. Geophys. Res. Space Phys.* **117**, 1–14 (2012).
 24. Delamere, P. A. & Bagenal, F. Solar wind interaction with Jupiter's magnetosphere. *J. Geophys. Res. Space Phys.* **115**, 1–20 (2010).
 25. Mann, I. R. *et al.* Coordinated ground-based and Cluster observations of large amplitude global magnetospheric oscillations during a fast solar wind speed interval. *Ann. Geophys.* **20**, 405–426 (2002). doi:10.5194/angeo-20-405-2002
 26. Rae, I. J. *et al.* Evolution and characteristics of global Pc5 ULF waves during a high solar wind speed interval. *J. Geophys. Res. Space Phys.* **110**, 1–16 (2005).
 27. Khurana, K. K. & Kivelson, M. G. Ultralow frequency MHD waves in Jupiter's middle magnetosphere. *J. Geophys. Res.* **94**, 5241 (1989).
 28. Wilson, R. J. & Dougherty, M. K. Evidence provided by galileo of ultra low frequency waves within Jupiter's middle magnetosphere. *Geophys. Res. Lett.* **27**, 835–838 (2000).
 29. Hasegawa, H. *et al.* Transport of solar wind into Earth's magnetosphere through rolled-up Kelvin-Helmholtz vortices. *Nature* **430**, 755–758 (2004).
 30. Ma, X., Stauffer, B., Delamere, P. A. & Otto, A. Journal of Geophysical Research : Space Physics Asymmetric Kelvin-Helmholtz propagation at Saturn ' s dayside magnetopause. *J. Geophys. Res. Space Phys.* **120**, 1867–1875 (2015). doi:10.1002/2014JA020746.Received
 31. Bonfond, B. *et al.* Quasi-periodic polar flares at Jupiter: A signature of pulsed dayside reconnections? *Geophys. Res. Lett.* **38**, 1–5 (2011).
 32. Nichols, J. D. *et al.* Response of Jupiter's auroras to conditions in the interplanetary medium as measured by the Hubble Space Telescope and Juno. *Geophys. Res. Lett.* **44**, doi:10.1002/2017GL073029 (2017).
 33. Sinclair, J. A. *et al.* Independent evolution of stratospheric temperatures in Jupiter's northern and southern auroral regions from 2014 to 2016. *Geophys. Res. Lett.* **44**, 5345–5354 (2017).
 34. Leahy, D. A. *et al.* On searches for pulsed emission with application to four globular cluster X-ray sources-NGC 1851, 6441, 6624, and 6712. *Astrophys. J.* **266**, 160–170 (1983).

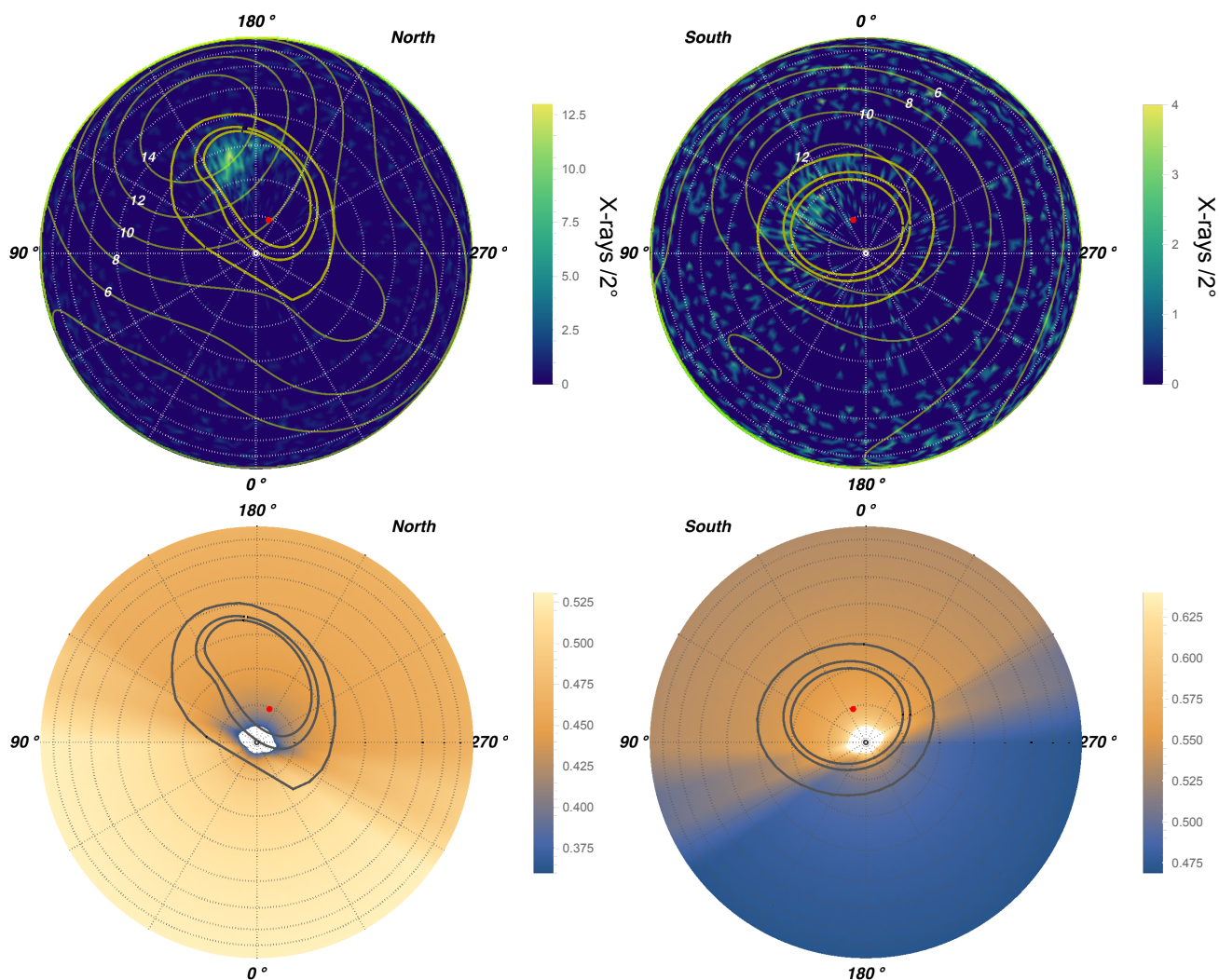


Figure 1: Upper: Polar Projections of Jupiter's Northern and Southern X-ray Aurora Projections centred on Jupiter's North (Left) and South (Right) poles. The projections combine 11-14hr X-ray observations of Jupiter on 24th May and 1st June 2016. Colours indicate the number of X-rays observed with the Chandra X-ray Observatory (CXO) High Resolution Camera (HRC) in bins of 1.5° by 1.5° of S3 latitude-longitude. Dotted lines of longitude radiate from the pole, increasing clockwise (anti-clockwise) for the North (South) pole in increments of 30° from 0° at the bottom (top). Concentric dotted circles outward from the pole represent 80°, 70° and 60° latitude. Thin gold contours with white text labels indicate the VIP4¹⁴ model magnetic field strength in Gauss. Thick gold contours show the magnetic field ionospheric footprints of field lines intersecting the Jovigraphic equator at 5.9 R_J (Io's orbit), 15 R_J and 50 R_J^{12,13} from equator to pole respectively. The location of Jupiter's dipole magnetic pole is given by the red dot. These projections reveal that the X-ray aurora is clustered into a hot spot at both poles. The Northern spot is between 155° and 180° longitude and 60° and 75° latitude, as previously observed^{2,3,5,7,8}. The Southern spot is longitudinally broader (30°-75°) and poleward of 67° latitude, located closer to the geographic pole. Projection effects lead regions of 1.5° latitude by 1.5° longitude near the poles to appear longer in latitude than in longitude, which leads to the streak-like morphology. This is an artefact of the projection and not a physical feature.

Lower: North (left) and South (right) polar projection exposure maps. The colour bar indicates the fraction of the total observing time during which each region was observed. These show that the clustering of X-rays in the hot spots is not due to additional observation time in these regions.

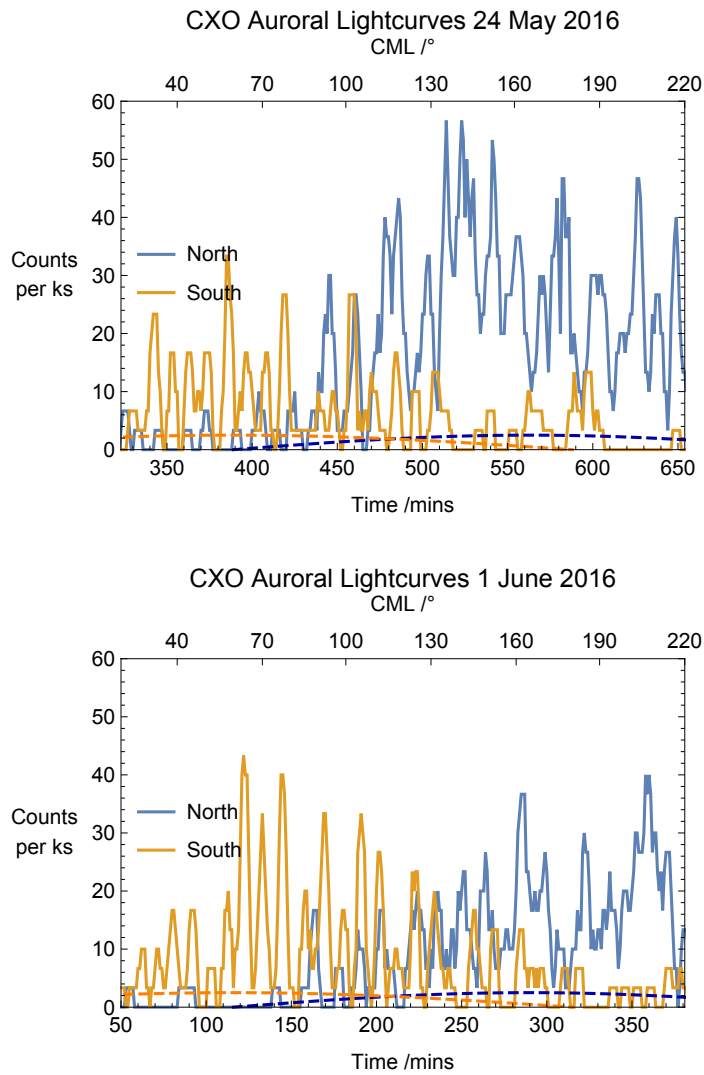


Figure 2: X-ray Aurora Lightcurves Chandra X-ray lightcurves from times when the Northern (blue) and Southern (gold) hot spots were both observable on 24th May 2016 (upper) and 1st June 2016 (lower). The visibility as a fraction of maximum visibility for the Northern (blue)/Southern (gold) hot spot is indicated by the dashed curves. Central Meridian Longitude is indicated across the top, while minutes from the observation start times (10:23 and 11:32 UT, respectively) are indicated on the x-axis. The lightcurves are 1-minute binned, with 6-minute moving-average smoothing.

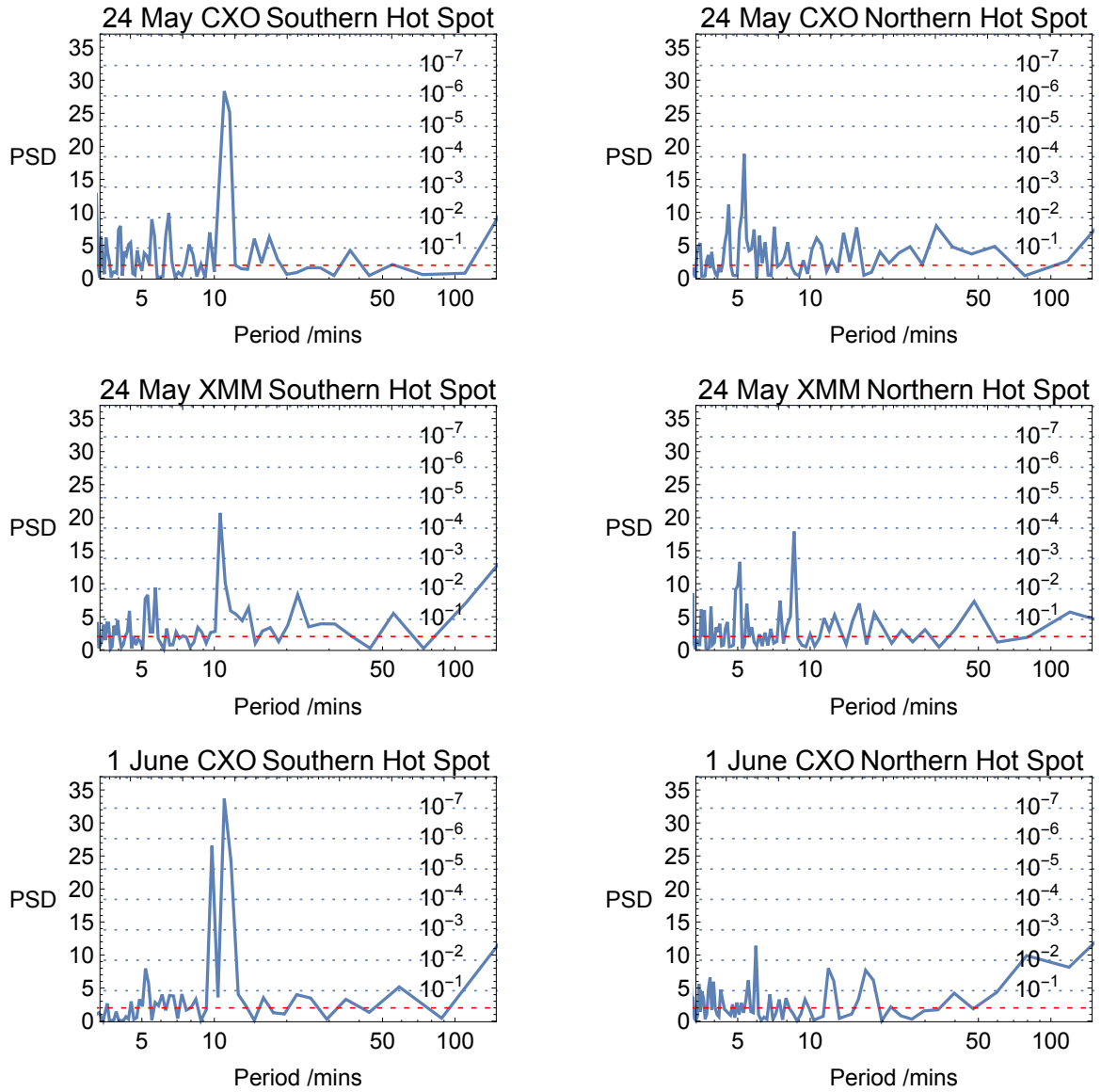


Figure 3: X-ray Aurora Periodograms Power Spectral Density plots from fast Fourier transforms of X-ray lightcurves from the Southern (left) and Northern (right) X-ray hot spots in 2016. PSDs are shown from Chandra observations on 24th May (upper), simultaneous XMM-Newton observations on 24th May (middle) and from Chandra observations 1st June (lower). The dotted horizontal lines show single-frequency probabilities of chance occurrence (PCO) for the detected periods³⁴. The lowest statistical significance and highest PCO of 10^{-1} is at the bottom of the plot. The dashed red line shows the value obtained if photons from a steady source were randomly distributed over the visibility period. Lightcurves were extracted from 20-70° longitude and poleward of -60° latitude for the South and from 155-180° longitude and poleward of 60° latitude for the Northern hot spot. For XMM, with poorer spatial resolution and therefore subject to increased contamination from the disk emission, the lightcurves are extracted from the same time window as the CXO observations.

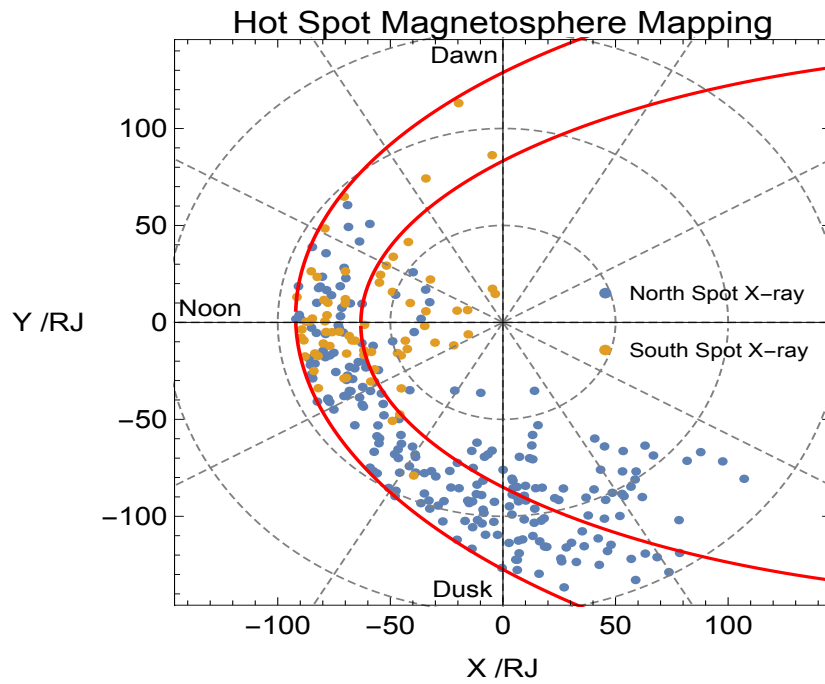
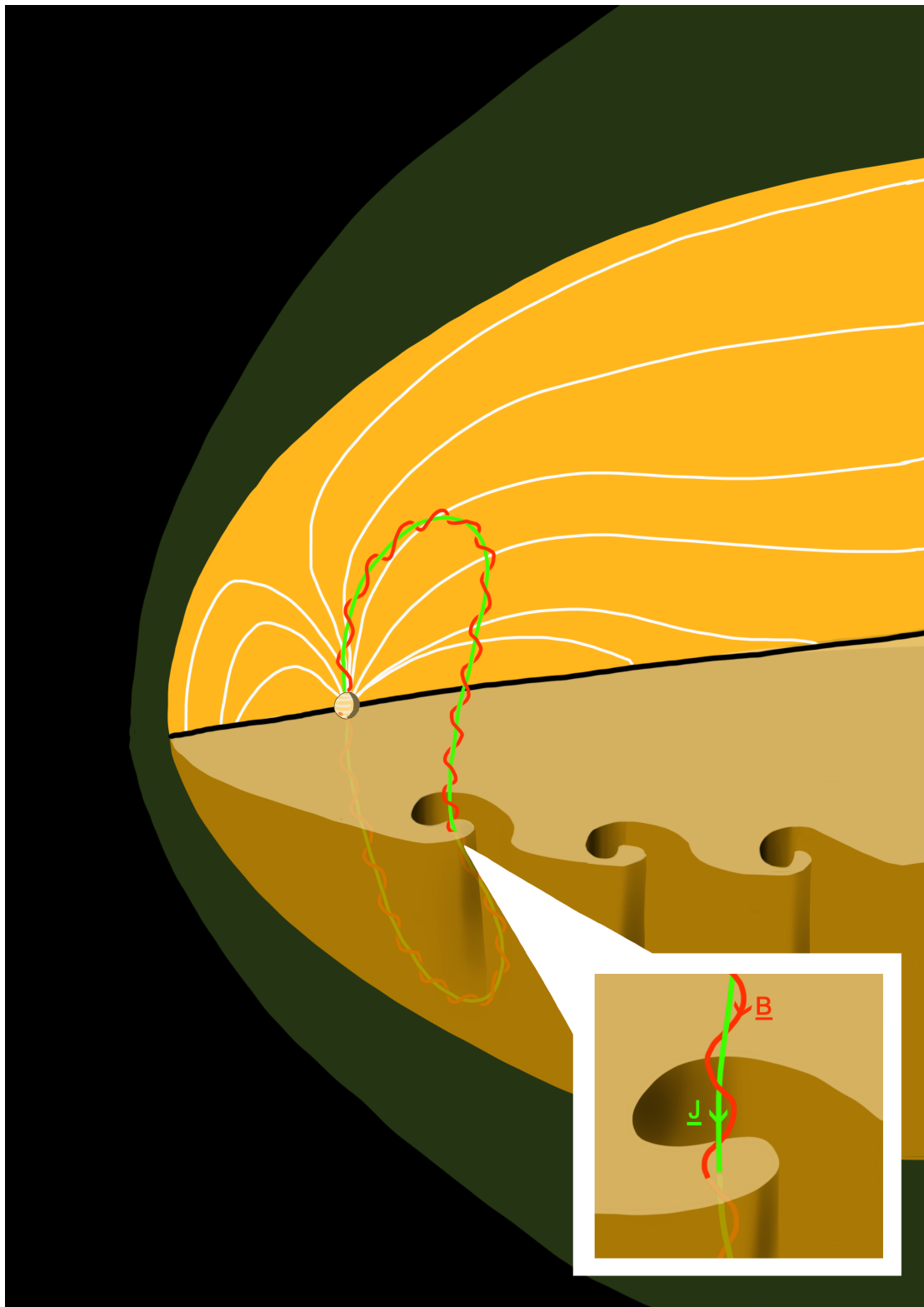


Figure 4: Upper: Ionosphere-Magnetosphere Mapping for the X-ray Hot Spots with Accompanying Schematic for a Kelvin Helmholtz Instability Driver Mapping¹³ of X-ray photon emission located in the ionosphere to the equatorial magnetosphere source regions for the Northern (Blue) and Southern (Gold) hot spots. The solid red lines indicate Jupiter's magnetopause¹⁶, for an expanded 92 R_J standoff distance (outer contour) and compressed 63 R_J standoff distance (inner contour). We also note that even for the statistical location of the expanded magnetopause, because of the substantial spatial extent of the hot spots, 30%-60% of X-rays mapped beyond the magnetopause, meaning that their origins cannot be identified by the model mapping and they are not plotted here.



Lower: An illustration of a possible source mechanism for the observed hot spot emissions. Kelvin Helmholtz Instabilities along the magnetopause could produce field line resonances that generate regular periodicity in the emissions. Further, these field line resonances could vary bi-modally with the compressed or expanded states of Jupiter's magnetosphere. These Kelvin Helmholtz instabilities may also generate non-conjugate North-South auroral signatures, since twisting of the magnetic field line (illustrated in red) can generate inter-hemispheric currents (green). Schematics for drivers relating to IMF B_Y -induced magnetic field line tension and high latitude reconnection can be found in the respective works^{18, 23}

Acknowledgements

WRD would like to thank N. Achilleos and R. Gray for very helpful discussions on Jovian X-rays and J-U Ness and Rosario Gonzalez-Riestra for their extensive help with XMM-Newton observations and particularly Pedro Rodriguez for assistance in re-framing them to Jupiter-centred coordinates. We also thank S. Badman, B. Bonfond, E. Chané, G. Clark, P. Delamere, R. Ebert, A. Masters, J. Nichols, A. Otto, C. Paranicas, A. Radioti, E. Roussos and C. Tao for insightful and informative conversations on Jupiter's aurora at the Vogt/Masters and Jackman/Paranicas ISSI team meetings. We thank the very helpful and insightful comments of our referees which allowed us to greatly improve this work. WRD is supported by a Science and Technology Facilities Council (STFC) research grant to UCL and by European Space Agency contract no. 4000120752/17/NL/MH. IJR, GHJ, GBR, AJC are supported by STFC Consolidated Grant to MSSL ST/N000722/1. IJR is supported by NERC grants NE/L007495/1, NE/P017150/1, and NE/P017185/1. GAG is supported by a UCL IMPACT studentship and the European Space Agency. CMJ is supported by a Science and Technology Facilities Council Ernest Rutherford Fellowship ST/L004399/1. MFV is supported by the National Science Foundation under Award No. 1524651. ZY is a Marie-Curie COFUND postdoctoral fellow at the University of Liege. Co-funded by the European Union. GRG would like to thank SAO for award GO6-17001A to SwRI. JAS and GSO acknowledge support from National Aeronautics and Space Administration to the Jet Propulsion Laboratory, California Institute of Technology. RCC acknowledges support from acknowledge support from Universidad Pontificia Comillas de Madrid-ICAI and Universidad Complutense de Madrid-Facultad de Informática This work is based on observations from the NASA Chandra X-ray Observatory (Observations 18608, 18609 and archival observation 8219) made possible through the HRC grant (NAS8-03060) and observations from the XMM-Newton Observatory (Observations 0781830301 and 0781830601). We warmly thank the Chandra and XMM-Newton Projects for their support in setting up the observations

Author Contributions

All authors were involved in the writing of the paper and contributed comments, sentences or paragraphs.

WRD led the work, organised the XMM-Newton observations and conducted the majority of the analysis for both CXO and XMM-Newton data sets.

GBR provided extensive expertise on XMM-Newton and analysis for the XMM-Newton data.

LCR provided extensive knowledge of planetary Magnetospheric dynamics and critical review of the techniques applied along with extensive paper writing and code to support the analysis.

CMJ and RPK organised the Chandra observations and provided extensive critical review of the Chandra data analysis.

RFE provided an extensive and thoroughly invaluable suite of analysis tools for the CXO data.

IJR and ZY provided extensive expertise on auroral drivers, magnetospheric processes and periodicity and wrote several paragraphs of the paper.

MFV provided her invaluable model mapping to identify origins for the auroral emissions, alongside written contributions.

GRG provided extensive expertise on the Jovian auroral emissions unique to his experience with X-rays and UV. He was also PI of the 2007 Chandra observation reported here.

GHJ provided the sketch of the KHI mechanism that could produce the non-conjugacy we observe in the emissions and re-writes and comments for the paper. GSO and JAS triggered the initial analysis through detailed discussions and critical review combining IR and X-ray emissions from the South Pole, alongside written contributions.

PGF provided code to reduce data from CXO given ACIS instrument degradation, alongside written contributions.

GAG provided code to support mapping of emissions, alongside written contributions.

RCC provided statistical analysis tools for the timings, alongside written contributions.

AJC provided extensive knowledge of planetary magnetospheres and provided sentences, comments and corrections on the main text.

Method Section

Observation Times

For all previously published X-ray campaigns with the Chandra X-ray Observatory^{2,3,5,7,8} (CXO) and XMM-Newton X-ray Observatory^{4,8,35,36} (XMM) the viewing geometry favoured observations of the Northern aurora. At these times, the sub-Earth latitudes of 0.2° - 3.9° and North Pole distance angles of 18° - 23° obscured visibility of the geographic South Pole (supplementary material). However, during Summer 2016 and March 2007 the tilt of Jupiter relative to the X-ray instruments in Earth orbit allowed clear X-ray observations of Jupiter's Southern geographic pole (North pole angle of -17° and -16° respectively and Sub-Earth Latitude of -1.7° and -3.3° respectively). It is this viewing geometry, which is rare in the legacy X-ray observations of Jupiter (see supplementary materials) that permitted clear observations of the Southern X-ray hot spot.

The 2016 CXO observations and XMM observation continuously observed a total Central Meridian Longitude (CML) range of 425° and 482° respectively during the 11.7 hour CXO observations (1.17 Jupiter rotations) and 12.3 hour XMM observation (1.23 Jupiter rotations). The CXO observations on 24th May and 1st June started with a Central Meridian Longitude (CML) of 185° and 350° respectively and finished with a CML of 250° and 55° respectively. The XMM-Newton observation on 24th May started with a CML of 175° and finished with a CML of 297° . The Chandra ACIS 3rd March 2007 5 hour observation covered a CML range of 290° - 110° . The entirety of Jupiter's disk fits within the field of view of both Chandra HRC and ACIS instruments and XMM-Newton's EPIC-PN instrument, permitting simultaneous observations of Jupiter's Northern and Southern hot spots during the CML window when both spots are at least partially on the observed disk. However, we note that the

Southern spot is rotating out of view when the Northern spot rotates into view, so that both spots can only be simultaneously observed in their entirety between CMLs $\sim 90^\circ$ - 120° and at these times there are still viewing geometry limitations and possible effects produced by the precipitation/emission-angle.

Given that each observation continuously covered 1.2 Jupiter rotations this meant that, for both observations, Jupiter's Northern and Southern hot spots were observed at least once, and the 24th May (1st June) observation partially observed Jupiter's Northern (Southern) hot spot a second time. To ensure that we did not artificially enhance the X-ray counts (lines 159-165 of the main text) by including multiple visits to the same spot (two visits to the North on 24th May and two to the South on 1st June), in each observation we extracted counts only from the longest duration window of these two possible observing windows. A table of the counts recorded by Chandra from every observing window can be found in the supplementary information.

Supplementary Figure 1 shows a projection onto the South Pole from the Chandra ACIS observation on 3rd March 2007. In order to analyse the ACIS data, we applied a correction to the effective area^{3,5} to account for the increased energy thresholds applied within ACIS to circumvent optical light leaks through the optical blocking filters. This observation had a lower observer co-latitude (Supporting Table 1), offering better visibility of the geographic South Pole than the 2016 campaign. Although the observations from the 2007 campaign were dimmer than those from 2016 and used a different instrument (Chandra ACIS instead of Chandra HRC), the polar projection shows that the X-rays are again concentrated into the Southern hot spot and that this occurs from 70° latitude to the pole and between 30° - 60° S3 longitude. Studies of eight X-ray observations of the Northern Spot have shown that from observation to observation the hot spot expands and contracts centered on a persistent location^{3,8}. This may suggest that while the Southern spot is centered on the same location in 2007 and 2016, it also expands and contracts from this location. Alternatively, the apparent expansion in the 2016 observations may be a projection effect produced by the slightly poorer visibility of the region during the 2016 observations relative to the 2007 observations.

Supplementary Figure 2 quantifies the concentrations of X-rays shown in Figure 1 and Supplementary Figure 1. In the 2016 and 2007 observations the Southern hot spot occurred in the same longitude range, suggesting that it is a persistent feature of the Southern X-ray aurora. We contrast the count concentrations in the auroral zones with emission from fluoresced and scattered solar photons in Jupiter's equatorial atmosphere. This demonstrates that the distributions are not produced by transient variations in the solar X-ray flux. If this were the case then the disk distributions might be expected to match the auroral distributions and they do not. We also plot error bars on the count measurements, highlighting the significance of the spots longitudinal concentrations relative to the more uniform equatorial emission.

Spectral Analysis

We analysed the XMM-Newton EPIC-PN spectral data from May 24th to identify the source populations of the observed emissions. To do this, we applied the standard

High Energy Astrophysics software packages including XMM-SAS and XSPEC. XMM-Newton has lower spatial resolution than Chandra. To circumvent this, we utilised the information from Chandra (from the overlapping interval) on the spatial locations of the spots with visibility information from NASA JPL Horizons ephemerides data to select times that corresponded to CML ranges when the hot spots were on Jupiter's observable disk. For XMM, for the North (South) we extracted hot spot spectra from times when the CML ranges were 60° - 270° (300° - 170°). The time intervals outside of these windows were checked to ensure that the X-ray emission was evenly distributed across Jupiter's entire disk and no significant auroral concentrations were lost. Given the dynamic nature of the hot spots, we only used the longest observation window and did not combine the shorter partial observation windows with this. This disregarding of times when the hot spot was unobservable is an alteration from previous spectral studies^{35,37}, that allowed us to minimise contamination from scattered solar photons and provided a more accurate calculation of X-ray emission rates from the aurora only.

Using the standard XMM-SAS package, we then selected the appropriate source regions for the Northern and Southern aurora from a planet-centered image and extracted the relevant spectral products (spectral data from source region, spectral data from background region, effective area/auxiliary response and redistribution matrix files). To ensure there were sufficient counts to reliably fit models, we binned the data into 10-channel energy bins. Using the XSPEC modeling package, we then tested fits for a combination of different Gaussian lines and bremsstrahlung continuum to a non-background subtracted spectrum (Jupiter's disk blocks cosmic X-ray background emission⁵).

To distinguish between auroral emission and potential contamination in the polar region from solar photons fluoresced/scattered in Jupiter's atmosphere, we also extracted the Equatorial emission by using the same time window as the auroral emissions. Given the low count rates, we used an Equatorial spectrum that covered the times when either hot spot was observable (sub-observer longitude 300° - 270°). Modeling of the Equatorial spectrum showed clearly distinctive features from the auroral emissions, indicating that the auroral spectra were dominated by a different emission process (i.e. not fluorescence and scattering of solar photons).

A bremsstrahlung continuum was found not to give good fits for the Northern or Southern auroral emissions, suggesting that both observed hot spots are dominated by spectral lines from precipitating ions.

It was challenging to directly compare the Northern and Southern aurora due to the low count levels for the South, but both the North (supplementary table 6) and South (supplementary table 7) best fit models feature a prominent and well-defined O VII line centered on 568 eV and a high flux line in the region where a range of sulphur and carbon lines are present. Both aurora best-fit models also include a line at 430-470 eV where there are known C VI lines. Interestingly, Carbon is much more abundant in the solar wind than in Jupiter's magnetosphere so this could suggest some direct solar wind precipitation. However, we note that the 90% confidence errors on the fluxes for this specific line are 50% of the measured flux for the North and more than this for the South. This 430-470 eV line coincides with the lowest data point between 200-900 eV on the equatorial spectrum, suggesting that it is not

contamination from scattered solar photons, but is a part of the auroral spectrum. The equatorial spectrum (supplementary figure 5) does hint at the presence of a line at 400 eV and we attempted to force model fits to this but these always led to worse fits and increased the reduced χ^2 by at least 0.5.

As with previous Jovian disk analysis³⁸, we could attain a good fit (reduced χ^2 of ~ 0.7) to the equatorial spectrum from 500-1500 eV with a vmekal hot plasma model using solar abundances and $kT \sim 0.3$ and flux of $\sim 9 \times 10^{-7}$ photons $\text{cm}^{-2}\text{s}^{-1}$. To support comparison with the auroral emission (supplementary figure 5), we show a spectral line fit with known solar spectrum lines³⁹ this shows that the equatorial emission has a very different structure above 600 eV. If the observed and modeled auroral emissions were due to solar contamination, then one would not expect the auroral emissions to decrease above 600 eV, as they do.

Given that both the Northern and Southern aurorae feature similar Sulphur/Carbon and O VII lines, this may support a similar source population (as suggested by the magnetospheric mapping to the noon magnetopause). This may also suggest that any independent behaviour is locally driven.

The Northern aurora is better fit with the inclusion of an OVIII line. More energy is required to strip the additional electron in order to produce this line, so the presence of the extra line may hint that a more energetic pulsation process occurs in the observable Northern aurora than in the South. This higher charge state oxygen would, through charge exchange, subsequently lead to a cascade of emissions from lower charge state oxygen, which may explain further differences between the oxygen spectra.

We note that the source regions for the two spectra are different (see Fig. 4), which may explain some of the spectral differences (acceleration, the driver process or the source ion population may change when moving from the nose to the dusk flank) and the spectra do not cover the same time interval. However, from this single North-South spectral comparison, it is difficult to quantify conclusively the differences between the two spectra, since the intensities of the Southern spectral lines are a factor of 2-4 lower than for the North. Future observations that provide good visibility of both poles will help to address and interpret the spectral characteristics with more statistical certainty.

Lightcurves and XMM-Newton Periodicity Detection

For Chandra, the 1-min binned lightcurves (Supplementary Fig. 2) from the Northern spot were produced by extracting X-rays from 155° - 190° longitude and poleward of 60° latitude. For the South, the 1-min binned lightcurves (Supplementary Fig. 2) were extracted from 20° - 70° longitude and poleward of -60° latitude. The 1-min binned unsmoothed data were then Fast Fourier transformed to produce the PSDs shown in Fig 4 of the main text. The lightcurves shown in main text figure 3 and supplementary figures 3 and 4 have been smoothed with a 6-minute moving. As with previous work^{2,3,5}, no moving-average smoothing was applied to generate the Fourier transform frequency data. Supplementary figure 3 shows the complete Northern and Southern

auroral lightcurves for the 24 May (Chandra and XMM-Newton) and 1 June (Chandra) 2016.

The lightcurves from XMM-Newton's European Photon Imaging Camera (EPIC) contain more noise than the Chandra HRC lightcurves because EPIC's lower spatial resolution leads to additional contamination from fluoresced and scattered solar X-ray photons on Jupiter's disk. This limited spatial resolution also prevents lightcurves from being extracted based on System III coordinate locations. As with the spectra, we therefore extracted XMM-Newton auroral lightcurves from the auroral region, during the same time window as the spectra - times when longitudes connected to the X-ray hot spots were observable (CML 60°-270° or 300°-170° for the Northern and Southern aurora respectively). The XMM-Newton Southern (Northern) Power Spectral Densities shown in main text figure 4, were therefore produced from fourier transforms of the 300-500 minute (450-700 minute) unsmoothed data that generated these lightcurves. The lightcurves for XMM-Newton are noisier, since the spatial resolution is not as good as Chandra's and it was therefore not possible to select areas in S3 coordinates. Instead, we used auroral regions extracted from the disk of Jupiter, which will include additional contamination from the disk emission. There are also different energy-dependent responses and effective areas for XMM-Newton's EPIC and Chandra's HRC and ACIS instruments, which may lead to differing lightcurve morphology for each instrument.

Jupiter's equatorial emissions are produced by solar photons that are fluoresced and scattered in Jupiter's atmosphere^{38,40,41}. Lightcurves and PSDs from the Jovian equator on 24 May (DoY 145) and 1 June (DoY 153) (Supplementary figure 4) between -30° and 30° latitude demonstrate that the periodic behaviour is not present in the equatorial region and that there was not a significant variation in the solar X-ray output (e.g. significant solar flares) during the observations^{3,38,41}.

To statistically test how similar the PSDs were between each pole, each instrument and each observation, we conducted a range of hypothesis tests and calculated the P-value⁴² for each compared data set. Direct comparisons of a hot spot PSD from the same pole but in different observations/instruments produced relatively high P-values (Supplementary Table 4), suggesting that the temporal behaviours of the emissions were similar. However, directly comparing the Northern PSDs with the Southern PSDs produced low P-values, suggesting the inter-hemisphere temporal behaviour is far less similar.

Supplementary Table 5 shows results from statistical analyses using the STA/LTA algorithm⁴³ to identify and characterise the 3 most prominent peaks in the power spectral density plots in Fig. 4 of the main text. This auto-detection of the peaks in the periodogram quantifies and characterises the strong 9-11 min period observed in the Southern spot, which is not also observed in the Northern spot. We do however note that a 5-8 min period does appear to recur in the North.

Data Availability Statement

The data analysed within this paper are publicly available from the Chandra and XMM-Newton Data Archives.

Bibliography for Method Section

35. Branduardi-Raymont, G., Elsner, R. F., Gladstone, G. R. & Ramsay, G. First observation of Jupiter by XMM-Newton. *Astronomy. Astrophys.* **337**, 331–337 (2004).
36. Hui, Y. *et al.* Comparative analysis and variability of the Jovian X-ray spectra detected by the Chandra and XMM-Newton observatories. *J. Geophys. Res. Space Phys.* **115**, A07102 (2010).
37. Branduardi-raymont, G. *et al.* Thermal and Non-Thermal Components of the X-Ray Emission from Jupiter. *Progr. Theor. Exp. Phys.* **169**, 75–78 (2007).
38. Branduardi-Raymont, G. *et al.* Latest results on Jovian disk X-rays from XMM-Newton. *Planet. Space Sci.* **55**, 1126–1134 (2007).
39. Phillips, K.J.H.; Leibacher, J.W.; Wolfson, C.J.; Parkinson, J.H.; Fawcett, B.C.; Kent, B.J.; Mason, H.E.; Acton, L.W.; Culhane, J.L.; Gabriel, A. H. . No Title. *Astrophys J* **256**, 774–787 (1982).
40. Bhardwaj, A. *et al.* Solar control on Jupiter’s equatorial X-ray emissions: 26-29 November 2003 XMM-Newton observation. *Geophys. Res. Lett.* **32**, 1–5 (2005).
41. Bhardwaj, A. *et al.* Low- to middle-latitude X-ray emission from Jupiter. *J. Geophys. Res. Space Phys.* **111**, 1–16 (2006).
42. Selke, T., Bayarri, J. J. & Berger, J. O. Calibration of p-values for testing precise hypotheses. *Am. Stat.* **55**, 62–71 (2001).
43. Allen, R. Automatic phase pickers: Their present use and future prospects. *Bull. Seismol. Soc. Am.* **72**, S225-242 (1982).